JOURNAL OF THERMOPHYSICS AND HEAT TRANSFER
Vol. 7, No. 2, April–June 1993

Current Distribution in the Cathode Area of an Arcjet

P. Durgapal*
NASA Ames Research Center, Moffett Field, California 94034

A theoretical model of the electrode phenomena, leading to the computation of the current density distributions, arc spot temperature, spot size, sheath voltage, ablation velocity, and ablation rates, is put forward. Computations for an atmospheric arc, at load currents ranging from 800 to 3000 A, in 1) one segment, and 2) four segment electrode configurations, are conducted. Spot size seems to vary linearly with load current, ranging from 1.82 to 3.22 mm for a rotating arcfoot, as the load current is varied from 800 to 3000 A. Even with arcfoot rotation, spot temperatures are high enough to cause ablation of the electrode material. Computations for P = 50 atm and I = 6000 A reveal that arc rotation is even more essential in order to save the excessive material ablation. In order to achieve an acceptable level of material ablation at P = 50 atm and I = 6000 A, a rotational frequency of 300–400 Hz needs to be achieved.

Nomenclature

A_{rich} = Richardson's constant, A/m^2/K^2
$\boldsymbol{B}$ = magnetic field strength, T
C_D = drag coefficient
c = specific heat, J/kg
$\boldsymbol{E}$ = electric field vector, V/m
e = electronic charge, C
F = heat of ablation, J/kg
I = load current, A
$\boldsymbol{J}$ = current density vector, A/m^2
j = current density, A/m^2
K = thermal conductivity, W/m/K
k = Boltzmann constant, J/K
$\dot{m}$ = total mass flow, kg/s
m_i = mass of ions, kg
N = number density, no./m^3
P = pressure, atm
R = inner radius of the electrode, m
R_s = radius of the spot, m
r = radial coordinate
s = electrode pitch, m
T = temperature, K
u = local gas velocity, m/s
V_a = ablation velocity, m/s
V_c = sheath voltage, V
v = average gas velocity, m/s
$\dot{W}$ = ablation rate, g/s
z = axial coordinate
ε_w = reflectivity of the wall
μ_0 = permeability of free space, H/m
ρ = density, kg/m^3
σ = electric conductivity, mho/m
$\phi_i(\phi_I)$ = ionization (excitation) potential, eV
ϕ_w = work function, eV
ψ = stream function
ω = relaxation parameter

I. Introduction

AN electric arc is a discharge of electricity between electrodes in a gas or vapor, with characteristic cathode or anode voltage drop at the electrodes. An arc at atmospheric pressure and above is characterized by a small intensely brilliant core surrounded by a comparatively cooler region of flaming gases. The core is at such high temperatures that all gases are completely dissociated. The current density at the cathode of an arc is very large and is practically independent of the arc current. It depends only on the material of the cathode, especially on its thermionic emission characteristics. The electrode material most commonly used is copper or copper alloy with high thermal conductivity to assure an adequate heat transfer rate capability.

Due to the high temperature of the arc spot, the electrode material at that location melts or sometimes instantaneously vaporizes, releasing electrode material and contaminating the flowing gas. Methods to reduce contamination from electric arc include 1) arcfoot rotation by vortex generation or magnetic field interaction; 2) selecting electrode material that can attain high levels of thermionic emission at relative lower spot temperatures; and 3) selecting electrode material with a high melting point.

Ames Research Center is currently operating a variety of arc-heated facilities. Of interest here is the segmented arc heater. The main components of a typical facility include a constricted arc heater, several interchangeable Mach number nozzles, a walk-in test chamber, and ancillary subsystems consisting of a steam-ejector vacuum system, cooling water system, and automated data acquisition system. The two electrodes are located on either side of the constrictor. The anode forms the upstream electrode and the cathode forms the downstream electrode. An electrode package consists of multiple rings that are the actual electrodes and each active electrode ring is insulated from the others by insulator rings and is individually ballasted. Each ring electrode has a given current rating. Electrodes are added to the stock until the number of electrode rings can handle the total current expected in the arc column. With proper adjustment of the individual ballasts, the electrode rings can be made to share current more or less equally. For the purpose of this study, it is assumed that future high-pressure and high-enthalpy arcjets will have similar configurations, with variations in electrode number and size.

In the first part of this article, a theoretical model of the electrode phenomena in arcjets is developed. The model consists of the following:

1) An axisymmetric model describing the electrical characteristics in the downstream electrode region (cathode) of an arcjet: The basic equations used are Maxwell's equations and the generalized Ohm's law. These, together with the necessary boundary and subsidiary conditions (typical of the electrode region) are then solved using the Gauss-Seidel successive relaxation technique. Profiles for the stream function and the current density are obtained as a result of this analysis.

Presented as Paper 91-1385 at the AIAA 26th Thermophysics Conference, Honolulu, HI, June 24–26, 1991; received July 15, 1991; revision received Nov. 27, 1991; accepted for publication Nov. 27, 1991.

*Research Scientist, Eloret Institute, M/S 229-4. Member AIAA.

The gasdynamic motion of the gas flowing through the heater is not included in this model.

2) Theoretical model of the arc termination at the electrode wall: The arc, being an electric current carrying body, seeks the path of least resistance. The portion of the arc which branches out from the main arc column and rotates towards the electrode wall is called the arcfoot. The point at which the arcfoot terminates is considered to be that point on the electrode at which the computed current concentration is maximum. Also, it is hypothesized that as the arcfoot moves normal to the axial direction, under the Lorenzian force of an applied magnetic field, a steady state is reached when the magnetic force is in equilibrium with the aerodynamic drag on the arc. The model relates the ion and electron currents to the spot size and temperature using several energy balance equations.

3) Thermodynamics of arc heating: A simple model of the arc heating based on radiative and convective heat transfer is presented.

The results are presented in the second section. Current distribution and stream function profiles for single and multiple electrodes with varying load current are discussed. Computation for the arc spot radius, arc spot temperature, ablation rate, etc. have been made also for various values of load current. Results from arcfoot parameter computations are presented for two types of cases: 1) without arcfoot rotation; and 2) with arcfoot rotation.

In order to verify and validate the theory put forward, and the results emanating from it, initially all the computations were conducted for an operating pressure of 1 atm. Some of the computed values, such as the arcfoot rotation frequency, are then compared with available experimental data. Since the constructed model will be used to analyze high-pressure operating conditions (as a prelude to the next stage of this study) one case at $P = 50$ atm is also analyzed and the results presented.

II. Theory

A. Current Distribution

The arc that enters the cathode region from the constrictor column is characterized by an intense core of high temperature and high-current density, surrounded by a comparatively cooler region of flaming gases. The electrode has a large magnetic field coil to force arc termination and rotation. The electrode rings are made to equally share the current by adjusting the individual ballasts. At each ring of the electrode the arc terminates as an arcfoot. In reality this is a three-dimensional problem but for simplicity it is modeled in two steps. In the first step an axisymmetric current distribution is determined, assuming that current terminating at the electrode segment is uniformly distributed around the electrode perimeter. The analysis provides the axial and radial distribution of the current density showing spots of high-current concentration. It is near these spots of current concentration where an arcfoot is formed. The analysis of the arcfoot is the second step.

In the axisymmetric current distribution analysis, it is assumed that the electrical properties of the electrode region are functions of the radial and axial coordinates only. They also depend on the electrode pitch in the axial direction. The gas velocity and temperature depend on the radial and axial coordinates and the pressure is constant throughout. Maxwell's equations and Ohm's law are used as the governing equations for the plasma in the electrode region and are written as

$$\left.\begin{aligned} &\nabla \times \boldsymbol{E} = 0, \quad \nabla \cdot \boldsymbol{B} = 0, \quad \nabla \cdot \boldsymbol{J} = 0, \quad \nabla \times \boldsymbol{B} = \mu_0 \boldsymbol{J} \\ &\boldsymbol{J} = \sigma[\boldsymbol{E} + \boldsymbol{v} \times \boldsymbol{B} + (1/eN_e)\nabla p_e] \end{aligned}\right\} \quad (1)$$

where N_e is the electron number density and p_e is the electron pressure. To evaluate the current density distribution the conventional stream function concept[1] is used. The stream function ψ is defined as

$$J_z = \frac{1}{r}\frac{\partial}{\partial r}(r\psi), \quad J_r = -\frac{\partial \psi}{\partial z} \quad (2)$$

where J_z and J_r are the axial and radial components of the current density. Equations (1) and (2) lead to the following second order differential equation for the stream function:

$$\frac{\partial}{\partial r}\left[\frac{1}{r}\frac{\partial(r\psi)}{\partial r}\right] + \frac{\partial^2 \psi}{\partial z^2} - \frac{1}{\sigma}\frac{\partial \sigma}{\partial r}\left(\frac{\psi}{r} + \frac{\partial \psi}{\partial r}\right) - \mu_0 \sigma v \frac{\partial \psi}{\partial z} - \frac{1}{\sigma}\frac{\partial \sigma}{\partial z}\frac{\partial \psi}{\partial z} + \frac{\sigma}{eN_e^2}\frac{\partial N_e}{\partial r}\frac{\partial p_e}{\partial z} - \frac{\sigma}{eN_e^2}\frac{\partial N_e}{\partial z}\frac{\partial p_e}{\partial r} = 0 \quad (3)$$

The following substitutions are used to normalize this equation:

$$x = z/s, \quad y = r/s, \quad T_e' = T_e/T_0, \quad N_e' = N_e/N_0$$

$$p_e = kN_eT_e = kN_0T_0n_e'T_e', \quad \psi' = \psi/(I/2\pi R) \quad (4)$$

Distances are normalized with respect to the electrode pitch s, temperature and electron density are normalized with their respective values at the origin. The stream function is normalized with respect to $(I/2\pi R)$. The final normalized equation is written as

$$\frac{\partial^2 \psi'}{\partial y^2} + \frac{1}{y}\frac{\partial \psi'}{\partial y} + \frac{\partial^2 \psi'}{\partial x^2} - \frac{\psi'}{y^2} - P'\left[\frac{\psi'}{r} + \frac{\partial \psi'}{\partial y}\right] - Q'\frac{\partial \psi'}{\partial x} + R_N \Big/ \left(\frac{I}{2\pi R}\right) = 0 \quad (5)$$

where

$$P = \frac{1}{\sigma}\frac{\partial \sigma}{\partial y}, \quad Q = \frac{1}{\sigma}\frac{\partial \sigma}{\partial x} + \mu_0 s \sigma v$$

$$R_N = \frac{\sigma k}{eN_e'}T_0\left(\frac{\partial N_e'}{\partial y}\frac{\partial T'e}{\partial x} - \frac{\partial N_e'}{\partial x}\frac{\partial T_e'}{\partial y}\right)$$

To solve this equation, boundary conditions on the electrode surface and the insulating wall and subsidiary conditions which are characteristic of the electrode region are needed. They are as follows:

1) On the surface of the electrode (good conductor), tangential component of the electric field vanishes, i.e., $E_x = 0$

$$\frac{\partial \psi'}{\partial y} + \frac{\psi'}{y} - \frac{\sigma k}{e}T_0\left(\frac{2\pi R}{I}\right)\left(\frac{\partial T_e'}{\partial x} + \frac{T_e'}{N_e'}\frac{\partial N_e'}{\partial x}\right) = 0 \quad (6)$$

2) On the insulating wall, normal component of the current is zero, i.e., $J_y = 0$, or $\psi = \text{const}$.

3) The current which runs through an arbitrary surface S, crossing the flow ahead of the electrodes, is equal to the load current. This yields

$$\int_S \boldsymbol{J} \cdot d\boldsymbol{s} = I \quad (7)$$

This implies that

$$\left.\begin{aligned} \psi_R^{x_0} &= \frac{I}{2\pi R} \qquad x \le x_0 \\ \psi_R^{x_0+1} &= \frac{I - I_1}{2\pi R} \qquad x_0 \le x \le x_0 + 1 \end{aligned}\right\} \quad (8)$$

In general if there are l electrodes

$$\psi_R^{x_0+l} = \frac{I - I_1 - I_2 \ldots - I_l}{2\pi R}, \quad x_{l-1} \leq x \leq x_l \tag{9}$$

In reality there are several electrodes and they are ballasted to share the current equally i.e., $I_1 = I_2 = I_3$, etc. This additional subsidiary condition is employed when more than one electrode is considered.

4) It is assumed that at the entrance of the electrode region, the flow is axial. To enforce this, for a $n \times m$ grid system in the x and y directions, respectively, it is assumed that

$$\psi(1, j) = \psi(2, j), \qquad j = 1, m \tag{10}$$

5) As pointed out earlier, all the current is forced to terminate on the electrodes, i.e., all the stream functions corresponding to the last axial point are zero

$$\psi(n, j) = 0, \qquad j = 1, m \tag{11}$$

B. Arcfoot Parameters

The second step in the model is the analysis of the arcfoot, a termination point of the central arc column of a given electrode. Now it is assumed that the disk of uniform current distributon transforms into a spoke and terminates at a certain location on the electrode. The arcfoot seeks the path of least resistance and is expected to terminate at the point where the current distribution is maximum. Depending on the temperature of the spot, erosion of the electrode material may occur. In order to minimize the erosion of the electrode due to the current concentration, an axial magnetic field is applied to the arcfoot by a magnet coil built inside each electrode segment. The arcfoot rotates in a radial plane under the influence of the Lorentz force. For this study a single electrode is considered. There are no experimental data available for comparison. One has to judge the result by technical arguments.

The study of cathodes emitting in a "spot" mode has been done for MHD generators.[2] The physical model presented here for arcjet cathode phenomenon is based on the conservation of energy on, and in the vicinity of the cathode.

There are four characteristic zones in the neighborhood of the cathode: 1) cathode spot, 2) space charge region, 3) ionization region, and 4) the discharge region. There are no collisions in the space charge region and the electron temperature is undefined. In the ionization region atoms are ionized in two steps. The first step is from ground to intermediate excited state and the next step is ionization. The ion temperature T_i is assumed to be equal to the neutral temperature and both are assumed to be the same in the ionization and discharge region. In order to determine the electron temperature in the ionization region, it is assumed that the average energy of the electrons is less than the energy required for ionization from the first excited state, since this is the elastic collision with the smallest energy transfer from the electron to the atom and, therefore, the smallest mean free path. It may be assumed that the distribution of electrons with energy less than this energy will be such that the average energy will be one-half of this energy, i.e.

$$\tfrac{3}{2}kT_e = \tfrac{1}{2}e(\phi_i - \phi_I) \tag{12}$$

If the pressure in the ionization region is assumed to be the same as in the rest of the gas, then

$$(P/kT) = N = N_0 + N_I + N_i + (Te/T)N_e \tag{13}$$

If the electron temperature T_e is much larger than the ionization temperature, and the degree of ionization is greater than 30%, the sum $(N_0 + N_I)$ of neutral and excited state number densities can be neglected in Eq. (13) to give

$$N = N_i + (Te/T)N_e$$

It is assumed that the gas consists of singly ionized atoms only $(N_i = N_e)$. This yields

$$N_i = [1/(1 + \theta)]N \tag{14}$$

where $\theta = T_e/T$. Using Eq. (12) and the assumption that $T_i = T$, the temperature ratio can be expressed as

$$\theta = (T_e/T_i) = [e(\phi_i - \phi_I)/3kT_i] \tag{15}$$

The ions are created by electron collisions in the air in a region near the cathode. The electrons are thermionically emitted from the cathode. The same cathode voltage which accelerates the ions to the cathode also accelerates the thermionically emitted electrons from the cathode into this ionization region. If it is assumed that all ionization energy returns to the cathode and if electrons leaving the ionization region carry average energy into the discharge volume, then the conservation of energy in the ionization region leads to

$$j_e V_c - j_i \phi_i = (j_e + j_i)[(\phi_i - \phi_I)/2] \tag{16}$$

On rearranging, the ratio of ion and electron currents is obtained in the form

$$\frac{j_i}{j_e} \equiv \Gamma = \frac{V_c - \frac{1}{2}(\phi_i - \phi_I)}{\phi_i - \frac{1}{2}(\phi_i - \phi_I)} \tag{17}$$

The electron current is related to the spot temperature by the Richardson equation[3]

$$j_e = A_{\text{rich}} T_s^2 \exp[-(e\phi_w/kT_s)] \cdot \exp(4.389\sqrt{E}/T_s) \tag{18}$$

where the electric field E is in V/cm. The current distribution at different locations on the electrode is determined using the electromagnetic code. Electric field is determined at the location where current distribution is maximum, using the expression

$$\boldsymbol{E} = (\boldsymbol{J}/\sigma) - (1/enN_e)\nabla p_e \tag{19}$$

The contribution of $\boldsymbol{v} \times \boldsymbol{B}$ term in Eq. (19) vanishes since $\boldsymbol{v}$ is zero on the electrode surface. The ion current is given by random thermal current

$$j_i = \tfrac{1}{4}eN_i v_i, \quad v_i = \sqrt{8kT_i/\pi m_i} \tag{20}$$

Next the energy balance on the cathode surface is considered. Both kinetic and ionization energies are transferred to the cathode. A spot forms at the location where this transfer of energy occurs. The size and temperature of this spot are estimated from an energy balance between the heat transferred to the cathode by the ions and the heat transferred from the spot by conduction in the cathode. The energy conducted from the spot to the surrounding material is

$$4R_s K(T_s - T_w) \tag{21}$$

The energy required to maintain radiation energy because of the spot is

$$\pi R_s^2 \varepsilon_w \sigma(T_s^4 - T_w^4) \tag{22}$$

If there is no ion reflection at the cathode, then the energy carried by the ion flux is

$$j_i(V_c + \phi_i - \phi_w) \tag{23}$$

The energy carried by the electron current emitted by the spot is $j_e\phi_w$, and the energy transported by the flux of excited neutrals to the cathode is $j_I\phi_I$. In the absence of any mass transfer from the cathode, the energy balance at the cathode

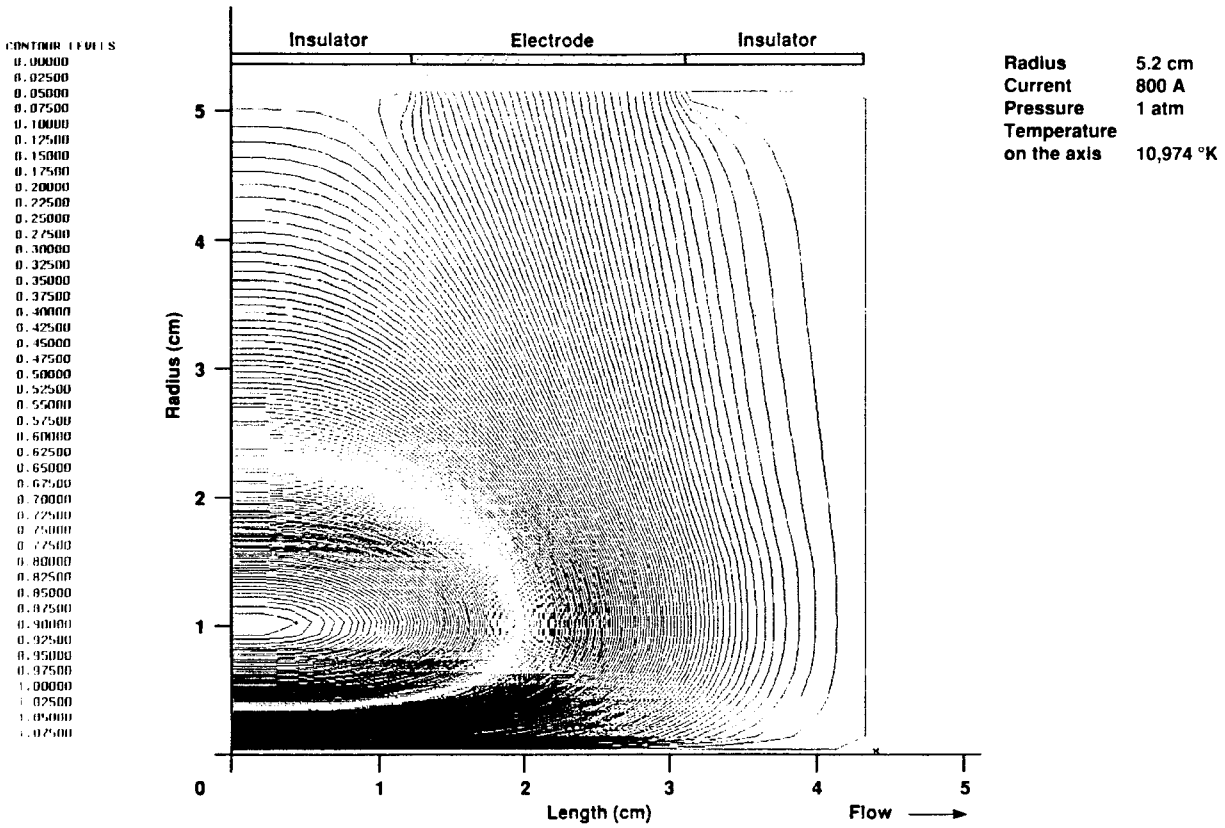

Fig. 1 Stream function distribution in a single electrode.

yields[2]

$$4R_sK(T_s - T_w) = \pi R_s^2[j_i(V_c + \phi_i - \phi_w) + J_I\phi_I - j_e\phi_w - \varepsilon_w\sigma(T_s^4 - T_w^4)] \quad (24)$$

The radius of the spot can be obtained from the expression of the total current

$$R_s = \sqrt{[I/\pi(j_e + j_i)]} \quad (25)$$

The nonlinear Eqs. (17) and (24) are solved simultaneously to yield the spot temperature and the sheath voltage. The radius of the spot is calculated from Eq. (25). When the spot temperature is greater than the melting point of the electrode material, then the total rate of material lost is calculated using a heat balance at the spot and is given by

$$\dot{W} = V_a\pi R_s^2\rho_m \quad (26)$$

If $V_a\rho_m F$ is the heat spent in melting or evaporating, as the case may be, and $V_a c\rho_m(T_s - T_w)$ is the heat spent in raising the temperature from T_w to T_s, then the ablation velocity is[4]

$$V_a = \frac{(q/A)_0}{\rho_m F\left[1 + \dfrac{c(T_s - T_w)}{F}\right]} \quad (27)$$

where $(q/A)_0$ is the heat flux to the arc spot, ρ_m is the electrode material density, T_w is the electrode wall temperature, and F is the heat of ablation. As pointed out earlier, the loss of electrode material due to current concentration is prevented by application of an axial magnetic field to the arcfoot by a magnet coil built inside each electrode segment. The arcfoot rotates in a radial plane under the influence of the Lorentz force. A steady state is reached when the magnetic force is balanced by the aerodynamic drag on the arc. In analogy with

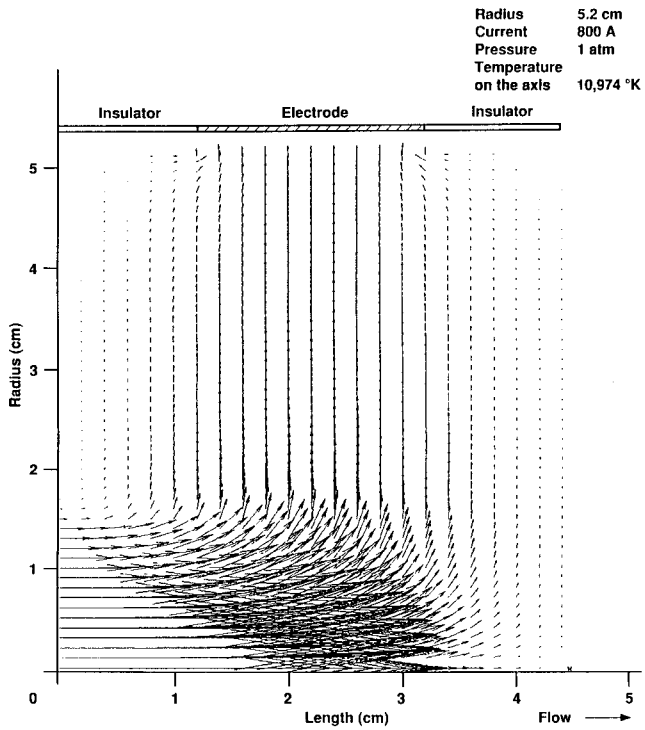

Fig. 2 Distribution of current density in a single electrode.

the drag coefficient on a solid cylinder in a flow, a drag coefficient can be defined as[5,6]

$$C_D = [IBL/\tfrac{1}{2}\rho_\infty v_a^2(2R_sL)] \quad (28)$$

where, ρ_∞ is the density of the surrounding gas, v_a is the velocity of the arc, R_s is the radius of the arc foot, and L is the length of the arcfoot. The rotation velocity of the arcfoot

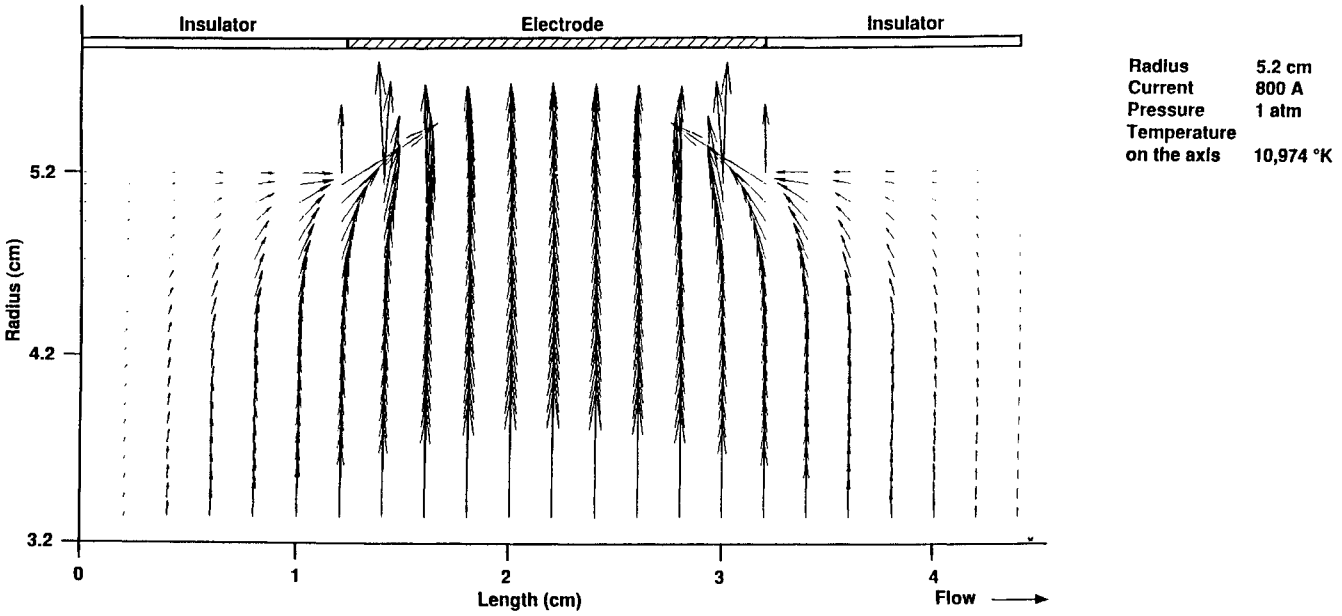

Fig. 3 Magnified view of current density near the electrode surface for a single electrode configuration.

is determined from Eq. (28). Experiments show that drag coefficient C_D can be approximated by using the drag coefficient of a rotating hot solid cylinder under similar fluid mechanical conditions. The variation of the drag coefficient with the Reynold's number is taken from Refs. 5 and 6. Reynold's number Re is based on the freestream velocity, density, diameter of the arcfoot, and the kinematic viscosity evaluated at the boundary of the arc and the surrounding gas.

C. Numerical Scheme

The axisymmetric equation for the stream function, together with all the boundary and subsidiary conditions, is then solved using the Gauss-Seidel successive relaxation technique. For calculation in the vicinity of the electrode, a small value of the relaxation parameter ω is used, because, at the electrode (due to strong current concentration) the solution cannot converge with values of $\omega \geq 1$. All derivatives are written using a central difference scheme.

It may be possible to use thermal properties from the program ARCFLO but ARCFLO has many uncertainties. For the present work, accuracy of the distribution of properties is not important. For this reason a much simpler model is used to compute the thermal properties, which takes the radiative and convective heat transfer in the electrode region into account (see Appendix).

III. Results

Validity of the arc heating model given in the Appendix is verified first. For $P = 1$ atm, $I = 1600$ A in a four segment electrode configuration (similar to the 60 MW facility at NASA Ames), thermodynamic properties in the radial and axial directions were computed. Other inputs for the computations were $\dot{m} = 0.131$ kg/s, $T_w = 1000$ K. From the anode through the constrictor, length is assumed to be 406.1 cm with a constant inner diameter of 4.0 cm. It is assumed that the transition ring of 3.3 cm joins four flat cylindrical ring pairs of electrodes and insulators of a constant diameter of 5.2 cm. Average enthalpy computed was 15.95 MJ/kg, which is in reasonable agreement with the experimental value of 17.9 MJ/kg reported by Winovich.[7] Total power supplied to the gas was 2.05 MW. Experimental data on radial distribution of temperature or enthalpy is not available.

A. Current Distribution

Electrical characteristics for different load currents and pressures in an arc heater are investigated. Computations are made for load currents between 800–3000 A at 1 atm pressure, and 6000 A at 50 atm. Some of the results are presented here. Two arrangements for the cathode region are considered. One consists of a single electrode with an insulating ring on either side. The other arrangement consists of four electrodes, each separated by a spacer ring, and there is a spacer ring at each end of the cathode region.

Figures 1 and 2 illustrate the stream function and current density distributions for a single electrode cathode region for $I = 800$ A and P = 1 atm. The thermodynamic data were generated by the heat transfer program with $T_w = 1000$ K, and $\dot{m} = 0.131$ kg/s as other inputs. In Fig. 1 it can be seen that the stream function has large values in the region enclosed by the first insulator ring. In the region covered by the electrode, the stream function starts to decrease and beyond this region it becomes very small. This occurs because all the arc current has terminated at the electrode. Figure 2 displays a vector plot of the corresponding current density distribution. It is evident from Fig. 2 that initially the current is concentrated near the axis (which is the core of the arc), then turns towards the electrode segment. Since in this simulation we have considered a single electrode, the current density distribution becomes insignificant on the right side (second insulator) very quickly. There seems to be a concentration of the current near the corners of the electrode which may cause excessive erosion near the ends. Figure 3 gives an amplified view of the current density distribution on and in the vicinity of the electrode surface. The magnitude of current density is 1.41×10^5 A/m^2, at the point of maximum current concentration.

For realistic modeling, an additional subsidiary condition based on the fact that several electrode rings are forced to share the current equally, is used. Figures 4 and 5 show the stream function and current density distribution for the cathode region with four electrodes for $I = 800$ A and $P = 1$ atm. The stream function is constant on the insulating rings and varies on the surface of the electrodes. Figure 5 shows how the current is equally shared by the four electrodes. This leads to a reduction in the current concentration on the electrode surface. The current density on the surface of the first electrode of the four electrode configuration is, 3.6×10^4 A/m^2, 3.9 times less than that for the single electrode configuration. This becomes more clear on taking a close up look at the first electrode and its neighboring insulating rings given in Fig. 6, and comparing it with Fig. 3. Increasing I from 800

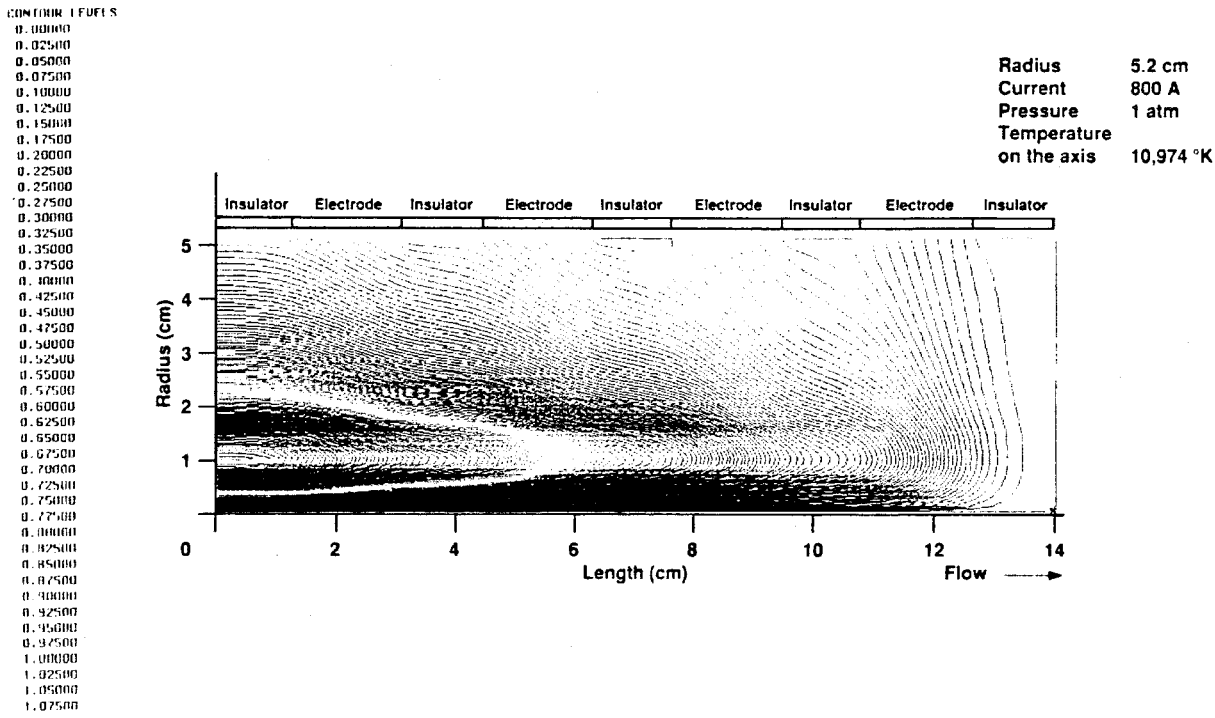

Fig. 4 Stream function distribution for a four electrode assembly.

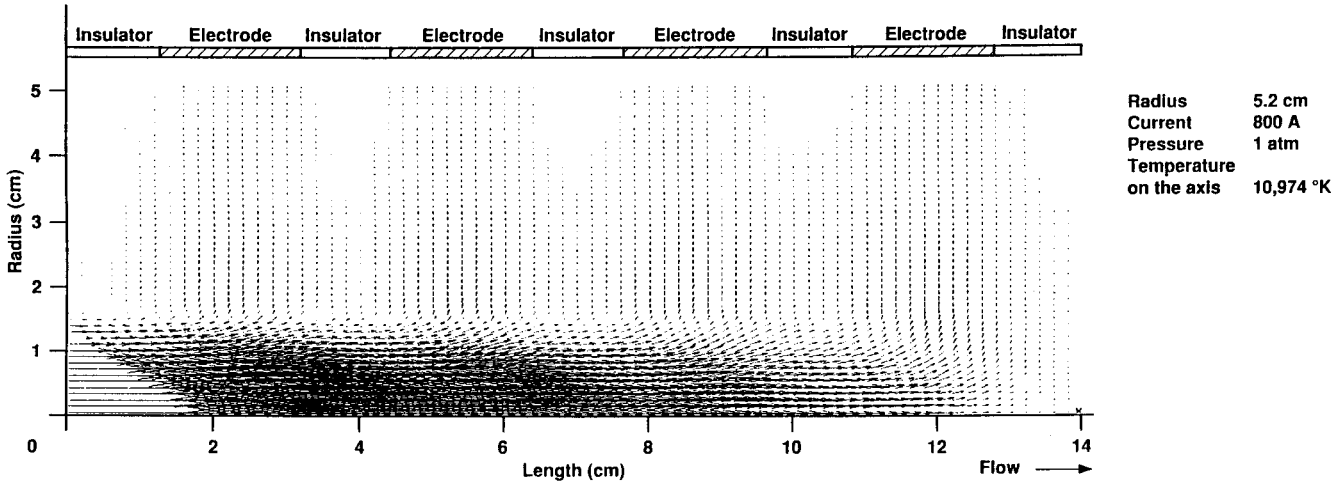

Fig. 5 Current density distribution for a four electrode assembly.

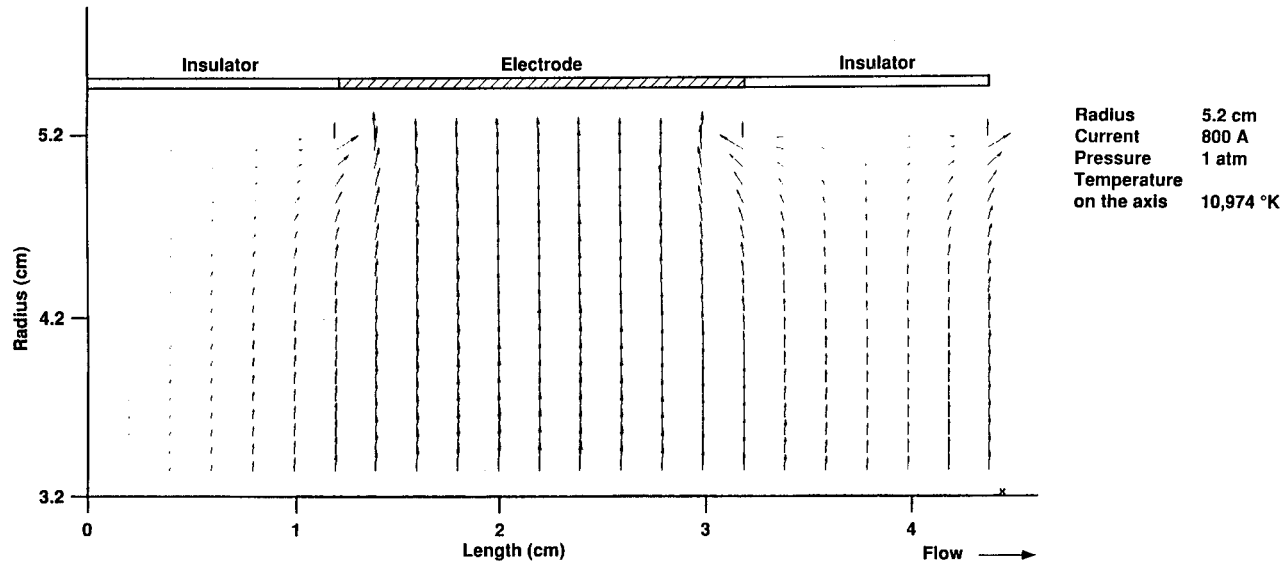

Fig. 6 Magnified view of current density near the first electrode of a four electrode assembly.

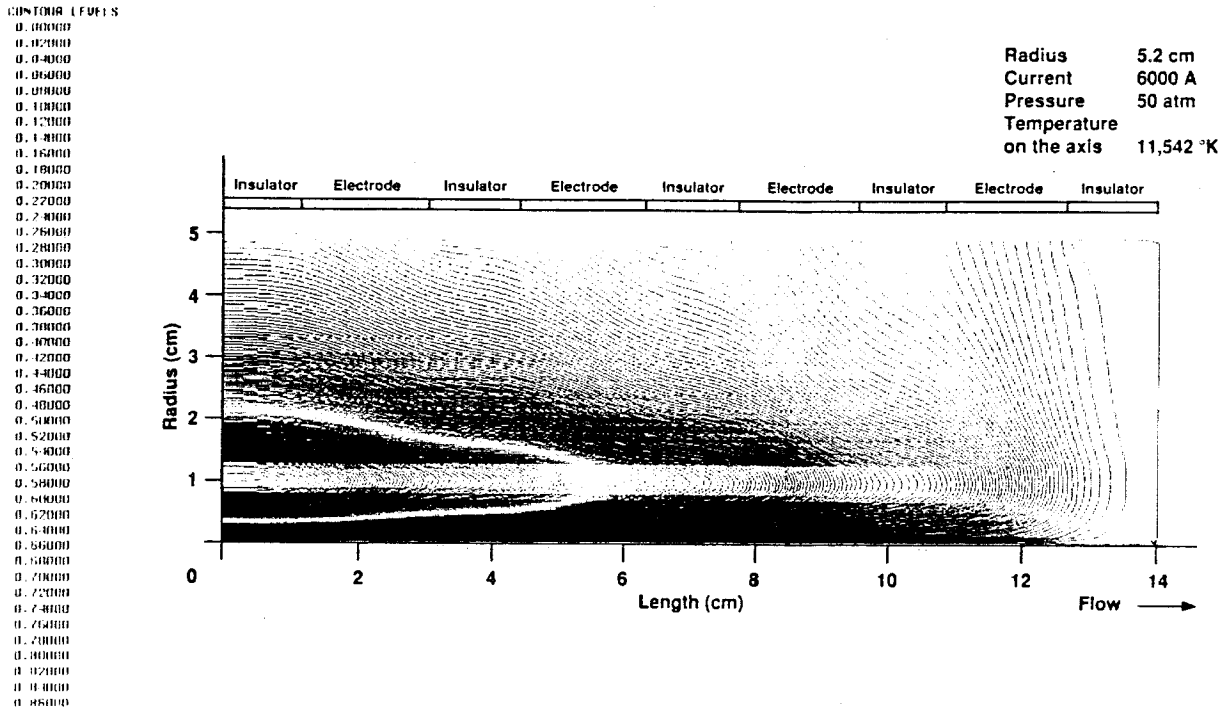

Fig. 7 Stream function distribution for a four electrode configuration at high pressure.

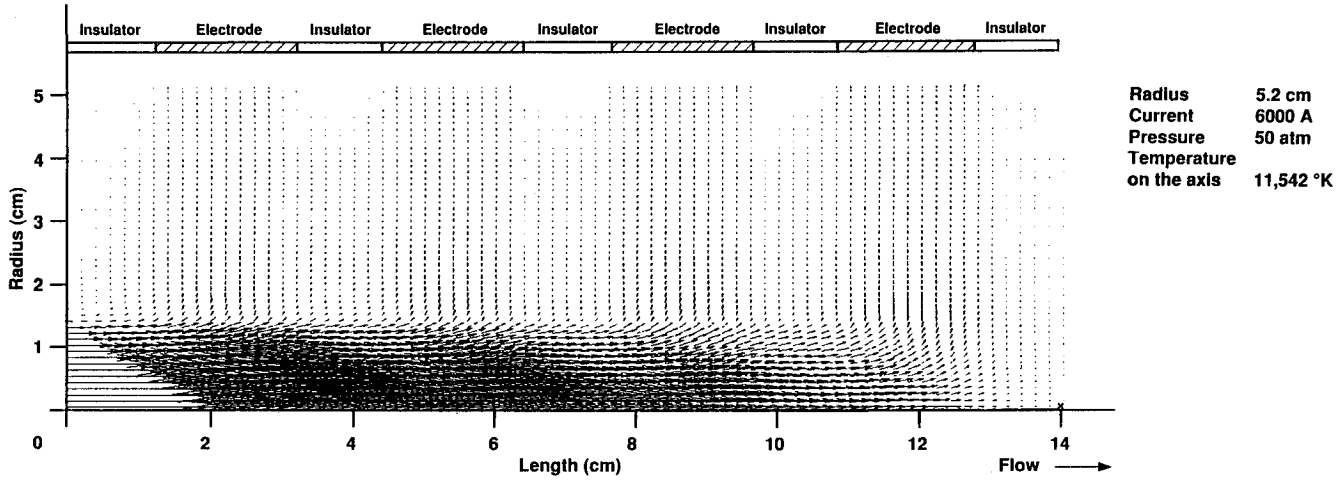

Fig. 8 Current density distribution for a four electrode assembly at high pressure. P = 50 atm, I = 6000 A, T_w = 1000 K, $\dot{m}$ = 3.0 kg/s.

to 3000 A leads to an increase in the current density by 3.69 times.

Figures 7 and 8 illustrate the electrical characteristics for a load current of 6000 A at 50 atm. For this case it is assumed that $\dot{m}$ = 3.0 kg/s, T_w = 1000 K. Total power deposited in the gas was 35 MW. The basic appearance of these plots does not seem to change significantly but the magnitude of the current density on the electrode surface are different. Also in this case, the current density for a one electrode configuration is 3.9 times more than that for a four electrode configuration. For a four electrode configuration the maximum current density at the wall is about 2.63×10^5 A/m^2. It is interesting to note that if one were to operate the arcjet at P = 1 atm with I = 6000 A, the maximum current density generated at the wall would be of the same order as it is for high-pressure operation P = 50 atm. However, the power deposited in the gas would be only 4 MW in the atmospheric arcjet as compared to the 35 MW of P = 50 atm operation.

B. Spot Parameters

In order to investigate the arcfoot parameters, a single electrode from the four electrode assembly is selected. For all

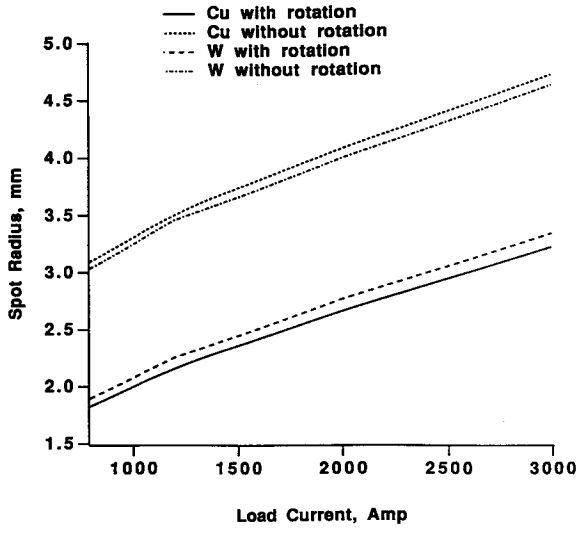

Fig. 9 Variation of spot radius with load current.

cases, arcfoot parameters for the second electrode are computed. Electric field is calculated at the point where the current density is maximum on this electrode. Spot parameters are computed for the atmospheric arc for load currents in the range 800–3000 A. Figures 9–11 illustrate the spot radius, spot temperature, and sheath voltage as a function of the load current. Each figure is shown for two electrode materials, copper and tungsten. In each case, results for stationary and rotating arcfoot are presented. Figures 9 and 10 show that as the load current increases, the spot radius and the spot temperature both increase. For copper, spot radius R_s increases from 1.82 to 3.22 mm when the load current is increased from 800 to 3000 A for a rotating arc. For stationary arcs, R_s increases from 3.09 to 4.72 mm for the same increase in load current. For tungsten, R_s increases from 1.89 to 3.34 mm for rotating arc, and 3.03–4.63 mm for stationary arc for the same load current. Thus, rotating the arc hinders erosion of the electrode surface. The sheath voltage (Fig. 11) decreases with increasing current, which is not very clear for the rotating arc case where it looks constant on the scale shown. The rotation frequency (Fig. 12) varies more or less linearly with the load current and is independent of the material of the electrode, as it depends only on the strength of the magnetic field. Figure 13 shows the ablation rate on the copper electrode surface. For stationary arcs this rate is much higher than that for rotating arcs. The same is true for ablation velocity (Fig. 14) which is of the order 0.01 mm/s for the rotating arc and of the order 1 mm/s for the stationary arc.

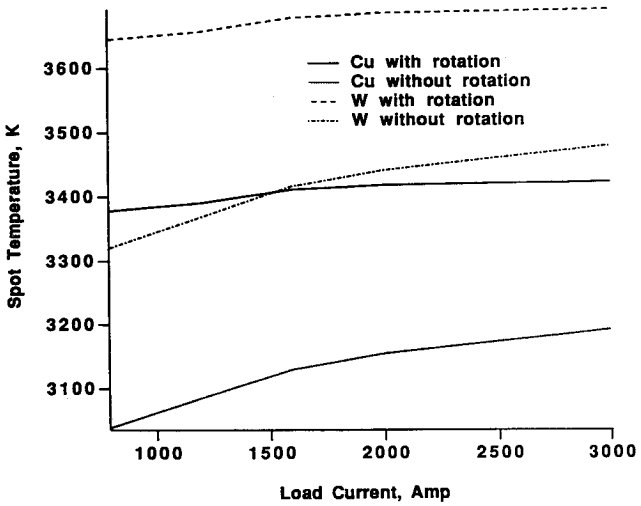

Fig. 10 Variation of spot temperature with load current.

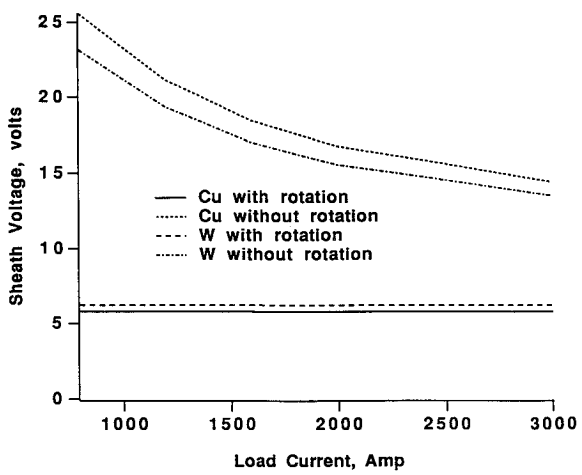

Fig. 11 Cathode voltage drop as a function of load current.

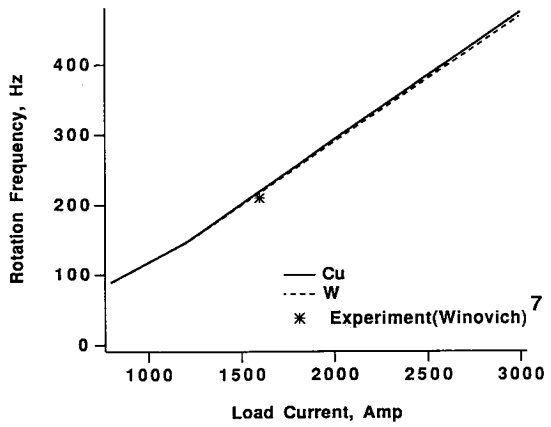

Fig. 12 Rotation frequency of the atmospheric arc as a function of load current.

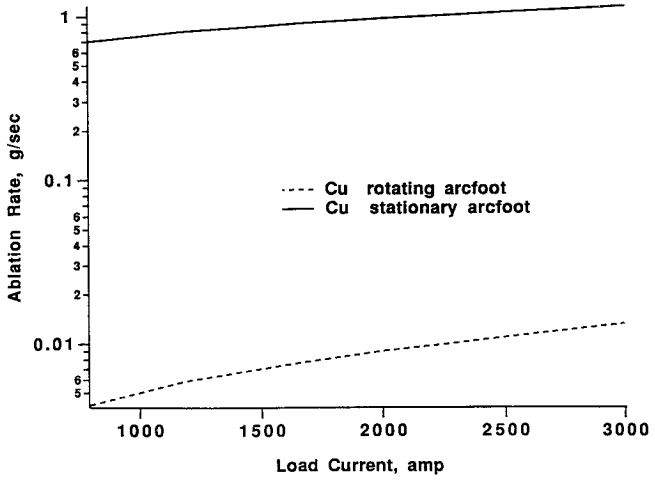

Fig. 13 Ablation rate on the surface of copper electrode as a function of load current.

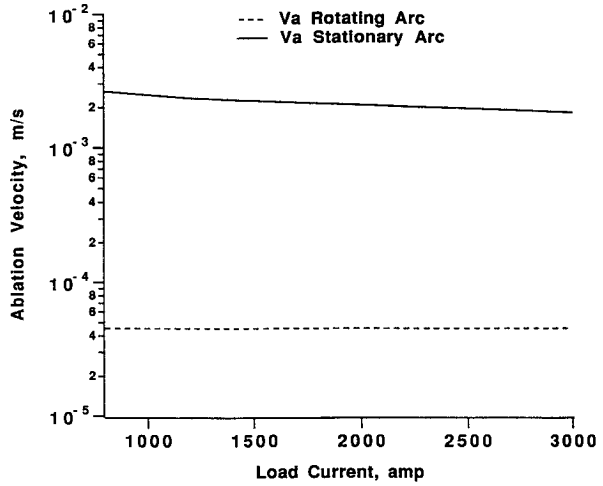

Fig. 14 Ablation velocity on the surface of copper electrode as a function of load current.

The computed arcfoot rotation frequency of 219.1 Hz for I = 1600 A in a four segment electrode configuration agrees well with the experimental value of 210 Hz measured by Winovich.[7]

The results for the high-current and high-pressure case are given in Tables 1 and 2 for the four and single electrode assemblies. In this case one value of current and pressure are considered. The spot size is small for both rotating and stationary arcs. This is true even when comparison is made with

Table 1 Arc spot parameters for $P = 50$ atm, $I = 6000$ A (four electrode configuration)

Material	f, Hz	R_s, mm	T_s, K	V_{sh}, V	V_a, m/s	A_{rate}, g/s
Copper	0.0	0.71	4453	6.7	1.7^{-2}	0.25
Copper	326	0.65	4537	5.7	6.0^{-5}	7.2^{-4}
Tungsten	0.0	0.72	4797	6.9	5.6^{-2}	1.8
Tungsten	321	0.67	4867	6.1	1.9^{-4}	5.4^{-3}

Table 2 Arc spot parameters for $P = 50$ atm, $I = 6000$ A (one electrode configuration)

Material	f, Hz	R_s, mm	T_s, K	V_{sh}, V	V_a, m/s	A_{rate}, g/s
Copper	0.0	1.36	4489	6.2	9.1^{-3}	0.47
Copper	1192	1.30	4532	5.7	6.1^{-5}	2.9^{-3}
Tungsten	0.0	1.4	4828	6.5	2.9^{-2}	3.4
Tungsten	1173	1.35	4864	6.1	1.9^{-4}	2.1^{-2}

the spot size at $I = 800$ A and $P = 1$ atm, which is about 1.82 for the rotating arc. However, the spot temperature becomes high, and is about 4500 K. Consequently, if the arcfoot is not rotated, extremely high ablation velocities are produced. If it is assumed that the magnetic field coil has same number of turns (4.5 turns), in the four segment electrode configuration, 0.65-mm spot will rotate with a frequency of about 321–326 Hz. Although in this high-pressure operation the Lorentz force is about 50 times larger than in the case of $I = 800$ A, $P = 1$ atm, the rotation frequency is only four times larger as the aerodynamic drag also becomes larger at high-pressure, high-current operation. The effect of rotation seems to be dramatic in this mode of operation. Rotation is absolutely a must at high pressure since the large ablation velocity for stationary arcs will result in deep erosion of the electrode. The ablation velocity for the rotating high pressure arc is 1.5 times that for rotating atmospheric arc while the ablation rate is about 10 times less ($I = 800$ A). These observations indicate that at higher pressure (in spite of higher spot temperature) total material loss will be less since the spot size is very small (provided the arc is allowed to rotate). At the present time no qualitative experimental data are available on ablation of the electrodes.

IV. Discussion

The current distribution analysis reveals that the arcfoot is likely to terminate at the left corner of the electrode segment, leading to excessive damage to the edge. In the present analysis, all the segments are assumed to be right-angle cylindrical rings, whereas in reality, the segments of NASA Ames arcjet facility are semicircular rings. Most likely such a configuration will provide more room for the current termination and therefore, smaller current densities. However, it requires a separate analysis with a semicircular configuration.

Inclusion of $\boldsymbol{v} \times \boldsymbol{B}$ force due to the induced field does not seem to significantly alter the current distribution ($v \sim 500$–700 m/s). However, if the mass flow through the arcjet is increased significantly, the affect of the induced field may become important.

Using tungsten electrodes may save the ablation of the material under certain load currents for the atmospheric arc; however, at high pressures, e.g., $P = 50$ atm, spot temperatures are such that even tungsten will vaporize instantaneously at the arc spot. At high pressure, the arc rotation seems to have even more dramatic effects, if one assumes that aerodynamic drag analogy for the arcfoot with a rotating hot cylinder holds for higher rotation frequencies (~300–400 Hz) also and Eq. (28) holds good.

At present, no reliable data on spot temperature, spot radius, sheath voltage, and ablation velocities, even for the present day operating conditions (~60 MW), are available. Therefore, an experimental program to systematically record data on such parameters, along with the theoretical analysis of high-pressure arcjets, will be launched in the very near future. Availability of such data will allow us to validate the present theoretical model and put more confidence in a future analysis.

V. Conclusions and Future Plans

In the first part of this article the stream function and current density distribution for an atmospheric arc with the load currents in the range 800–3000 A and for a 50 atm arc with the load current of 6000 A are calculated. In the second part, spot size, spot temperature, sheath voltage, rotation frequency, ablation velocity, and ablation rate for the same thermal and electrical conditions are computed. The current distribution analysis reveals that the arcfoot, termination point of the arc at the electrode wall, is drawn to the corner of the electrode ring. The spot size of the arcfoot increases linearly with the load current, varying from 1.82 to 3.22 mm if I is varied from 800 to 3000 amp for $P = 1$ atm for a rotating arcfoot. The spot temperatures are such that Cu electrode instantaneously vaporizes, adding material to the environment. If tungsten is used as the electrode material, ablation in some cases might be avoided. If the arcfoot is not allowed to rotate, the spot size almost doubles and the ablation rate increases by two orders of magnitude, for example, from 4.2×10^{-3} g/s to 7.0×10^{-1} g/s, for $I = 800$ amp, $P = 1$ atm operation. A nonrotating arcfoot is likely to destroy the electrode almost instantaneously.

At high pressures the spot size tends to be small even with high-load current but the ablation velocity is large. Rotation of the arcfoot becomes ever so important, as the ablation for a nonrotating arcfoot increases about 4000 times in comparison to a rotating arcfoot. Also, high pressure operation leads to larger ablation velocities, even in cases of rotating arcs. In the present article only one set of calculations are made for high current, high pressure arc. Therefore, at this point it is difficult to draw any definite conclusions. In a future article, more data will be generated and discussed.

Appendix: Thermodynamics of Arc Heating

The arc column is considered a central current carrying body at a uniform temperature, T_A and is the only source of ohmic heat. The bulk gas in the annulus surrounding the arc is heated by convective turbulent and radiative heat transfers. The arc column (in addition to heating the surrounding gas) loses energy directly to the tube (constrictor or electrode) wall by volumetric radiation. The arc and bulk gases are assumed to be optically thin. The bulk gas loses energy to the tube wall by turbulent convection. The temperature in the bulk gas is assumed to vary as

$$\frac{T - T_{Bm}}{T_A - T_{Bm}} = \left(\frac{u}{U}\right)^m, \qquad \frac{u}{U} = 1.0 - \left(\frac{r}{R}\right)^n \tag{A1}$$

where T is the bulk gas temperature at radius r, T_A is the arc temperature, T_{Bm} is the enthalpy averaged mean temperature

of the bulk gas, and R is the inner radius of the tube. The constants m and n have been taken to be 1 and $\frac{1}{7}$, respectively.

Energy balance per unit length of arc column is written by equating the electrical input energy to the energy lost by radiation to the surroundings, and by turbulent convection to the annulus bulk gas[8]

$$(j^2/\sigma)\pi D_A^2 = E_A(\pi/4)D_A^2 + \pi h(T_A - T_{Bm})D_A \quad \text{(A2)}$$

where $j = 4I/\pi D_A^2$ is the current density, with I being the load current, with D_A being the arc diameter, E_A is the volumetric radiative power output from the arc column, h is the convective heat transfer coefficient, and T_A and T_{Bm} are the arc and the mean bulk temperatures, respectively. E_A is computed by the Ames Research Center Radiation Program (ARCRAP4)[9] with the operating pressure P, arc temperature T_A and the corresponding equilibrium composition of air as input. The equilibrium composition of air at T_A is computed by NOZ2[10] computer code. The turbulent heat transfer coefficient is computed using the conventional formulation including the Nusselt number, Reynolds number, Prandtl number, mass flow, and tube hydraulic diameter.

Heat flux to the wall are from two sources: 1) radiative flux from the arc q_r; and 2) convective heat transfer from the bulk gas q_c. They can be expressed as

$$q_r = E_A(\pi/4)D_A^2 - \varepsilon_B T_{Bm}^4, \quad q_c = h(T_{Bm} - T_w) \quad \text{(A3)}$$

where ε_B is the gray gas emissivity computed at T_{Bm}, and T_w is the wall temperature. The energy contained in the gas is given by

$$\left.\begin{aligned} E_G &= h_A\dot{m}_A + h_B\dot{m}_B, \quad \dot{m}_A = \rho_A A_A v, \quad \dot{m}_B = \rho_B A_B v \\ v &= \frac{\dot{m}}{\rho_A A_A + \rho_B A_B} \end{aligned}\right\} \quad \text{(A4)}$$

where h_A and h_B are the enthalpies, ρ_A and ρ_B are the densities, A_A and A_B are the cross-sectional areas of the arc and annulus gas, $\dot{m}_A$ and $\dot{m}_B$ are the mass flows, respectively. $\dot{m}$ is the total mass flow through the tube and v is the gas velocity. The energy balance for the gas becomes

$$E_G = (j^2/\sigma)\pi D_A^2 L - \dot{m}h_i - \pi 2RL(q_r + q_c) \quad \text{(A5)}$$

where h_i is the enthalpy of the input gas and L is the total length of the constrictor or the electrode area. With the mass flow, load current, operating pressure, and the geometrical parameters of the tube as input, for an assumed arc diameter D_A, the temperatures T_A and T_{Bm} are determined by simultaneously solving Eqs. (A2) and (A5). The arc diameter D_A, for which the power input $(j^2/\sigma)\cdot\pi D_A^2$ is minimum, is taken to be the true solution.

Acknowledgment

This work was supported by NASA Grant NCC2-688.

References

[1]Ishikawa, M., "Study on Performance Characteristics of Diagonal Type Nonequilibrium Plasma MHD Generator," Inst. of Atomic Energy, Kyoto Univ., Kyoto, Japan, Feb. 1978, p. 37.

[2]Nichols, L. D., and Mantenieks, M. A., "Analytical and Experimental Studies of MHD Generator Cathodes Emitting in a "Spot" Mode," NASA TN D-5414, Sept. 1969.

[3]Cobine, J. D., "Emission of Electrons and Ions by Solids," *Gaseous Conductors*, 1st ed., Dover, New York, 1958, pp. 106–122.

[4]Rohsenov, W. M., and Choi, H., "Heat Transfer in Stationary Systems," *Heat, Mass and Momentum Transfer*, Prentice-Hall, Englewood Cliffs, NJ, 1961, p. 122.

[5]Winograd, Y. Y., and Klein, J. F., "Electric Arc Stabilization in Crossed Convective and Magnetic Fields," *AIAA Journal*, Vol. 7, No. 9, Sept. 1969.

[6]Roman, W. C., and Myers, T. W., "Experimental Investigation of an Electric Arc in Transverse Aerodynamic and Magnetic Fields," *AIAA Journal*, Vol. 5, No. 11, 1967.

[7]Winovich, W., "An Instrumentation System to Measure Arc Rotation Frequency," Rept. prepared for Ames Research Center, by FluiDyne Engineering Corp., Mountain View, CA, Nov. 1990.

[8]Painter, J. H., and Shaeffer, J. F., "Performance and Scaling Characteristics of a Huels-Type Arc Heater Operating on Hydrogen, Helium or Air," AIAA Paper 76-14, Washington, DC, Jan. 1976.

[9]Arnold, J. O., Cooper, D. M., Park, C., and Prakash, S. G., "Line-by-Line Transport Calculations for Jupiter Entry Probes," *Entry Heating and Thermal Protection*, edited by W. B. Olstad, Vol, 69, Progress in Aeronautics and Astronautics, AIAA, New York, 1980, pp. 52–82.

[10]Park, C., Howe, J. T., Jaffe, R. L., and Candler, G. V., "Chemical Kinetic Problems of Future NASA Missions," AIAA Paper 91-0464, Reno, NV, Jan. 1991.